

# STRUCTURE-AWARE ADAPTIVE KERNEL MPPCA DENOISING FOR DIFFUSION MRI

Ananya Singhal, Dattesh Dayanand Shanbhag, Sudhanya Chatterjee

GE HealthCare, Bengaluru, India

## ABSTRACT

Diffusion-weighted MRI (DWI) at high b-values often suffers from low signal-to-noise ratio (SNR), making image quality poor. Marchenko-Pastur PCA (MPPCA) is a popular method to reduce noise, but it uses a fixed patch size across the whole image, which doesn't work well in regions with different structures. To address this, we propose an adaptive kernel MPPCA (ak-MPPCA) that selects the best patch size for each voxel based on its local neighborhood. This improves denoising performance by better handling structural variations.

**Index Terms**— Diffusion MRI, MPPCA denoising, adaptive filtering, kernel optimization

## 1. INTRODUCTION

DWI is crucial for characterizing tissue microstructure, but high b-value acquisitions suffer from low signal-to-noise ratios (SNR). MPPCA has emerged as a popular approach for DWI denoising by leveraging random matrix theory to distinguish signal from noise [1]. Popularly this has been implemented in patch-based manner. Recently, investigations have been published which aim at improving aspects of MPPCA denoising. Henriques et al. explored threshold-based criteria for component selection [2]. Several works have evaluated tensor-based approaches for multi-dimensional data denoising using MPPCA [3, 4]. The emphasis has been on methods to improve the noise estimate. However, these methods employ fixed kernel sizes across entire volumes, which does not account for structural heterogeneity of the in-vivo image. Adaptive patching in MPPCA, as implemented in DE-SIGNER [5, 6] attempts to overcome this challenge by selecting voxels for denoising based on both spatial proximity and signal similarity.

In this work, we introduce adaptive kernel MPPCA (ak-MPPCA), a denoising approach that estimates the optimal kernel size for each voxel based on the structural complexity of surrounding tissue. Structural complexity is quantified using image gradient information, allowing the method to adapt locally to anatomical variation. This eliminates the need for manual kernel size tuning and improves denoising performance by preserving fine structural details.

## 2. METHODS

MPPCA uses principles from random matrix theory to separate signal from noise in DWI data [1]. It removes noise-dominated eigenvalue components by identifying those that fall within the bounds of the Marchenko-Pastur distribution, thereby preserving meaningful signal. However, conventional implementations use a fixed kernel size across the image, which fails to adapt to local tissue heterogeneity. In this work, we propose a voxel-wise adaptive kernel estimation strategy that adjusts the kernel size for denoising based on the structural complexity of each voxel's neighborhood.

### 2.1. Kernel Map Estimation

DWI data at a given b-value is typically represented as a 4D volume, where the fourth dimension corresponds to diffusion directions. In this section, we describe our method for estimating the optimal kernel size for each voxel to improve MPPCA-based denoising.

#### 2.1.1. Data Selection for kernel size estimation

To estimate voxel-wise kernel sizes for denoising, we use the trace image from the lowest available b-value image, provided that  $b \geq 100$ . This image is chosen because it is sufficiently diffusion-weighted to reflect tissue microstructure, while still preserving enough signal to capture structural complexity. This balance makes it suitable for guiding kernel size estimation.

#### 2.1.2. Gradient-Based Structural Characterization

To assess structural heterogeneity around each voxel, we compute the image gradient information ( $G$ ) as follows:

$$G = \sqrt{(S_x * (I * G_\sigma))^2 + (S_y * (I * G_\sigma))^2} \quad (1)$$

where  $S_x$  and  $S_y$  are the Sobel operators,  $I$  is the image selected as described in Section 2.1.1,  $G_\sigma$  is a Gaussian kernel with  $\sigma = 4$ , and  $*$  denotes convolution. Gaussian smoothing reduces noise sensitivity during edge detection. Voxels with high gradient values indicate complex tissue structures, while low gradient values suggest simpler or more homogeneous regions. Here,  $G$  has the same dimensions as  $I$ , a 3D volume

corresponding to a diffusion direction in the DWI data (see Section 2.1.1).

### 2.1.3. Kernel Size Determination

This section describes the method used to estimate voxel-wise kernel sizes for MPPCA denoising based on image gradient information. Since gradient magnitudes are floating-point values and kernel sizes must be odd integers, we propose an algorithm to map gradient values to discrete kernel sizes. The user provides a lower ( $k_l$ ) and upper ( $k_u$ ) bound for kernel size, both as odd integers. Let  $\{n_k\}_{k=1}^K$  denote the set of  $K$  plausible kernel sizes within the range  $[k_l, k_u]$ . Gradient values within the brain mask are clustered into  $n_k$  groups using the k-means clustering algorithm. The brain mask is generated using median Otsu thresholding as implemented in DIPY [7]. Voxels outside the brain mask are assigned a fixed kernel size  $k_h = H$ . In our work, we consider  $H = k_u$ . The clustered gradient image contains values  $\{g_{n_1}, \dots, g_{n_K}, g_h\}$ . We assume that for clusters  $g_{n_i}$  and  $g_{n_j}$ , if  $i < j$ , then  $\{G \in g_{n_i}\} > \{G \in g_{n_j}\}$ ,  $\forall \{i, j\}$ . For each voxel at location  $(x, y, z)$ , if  $G(x, y, z) = g$  and  $g$  belongs to the  $i^{\text{th}}$  cluster, then the assigned kernel size is  $k_i$ .

In summary, gradient values are grouped into clusters corresponding to the number of available kernel sizes. Voxels with higher gradient magnitudes receive smaller kernels, while those with lower gradients are assigned larger kernels. This results in a voxel-wise kernel size map with odd integer values, matching the dimensions of the gradient image. For this work, we consider kernel sizes to be isotropic. The algorithm has been shown in Algorithm 1.

## 2.2. ak-MPPCA: MPPCA with estimated kernel size

The MPPCA implementation is updated to consider the estimated kernel size for patch based denoising across the voxels. The remaining aspects of MPPCA denoising, such as noise estimation and signal thresholding is maintained as discussed in Veerart et al. [1]. In this work, we set  $k_l$  and  $k_u$  to 5 and 9 respectively.

## 2.3. Data and Experiment

All evaluations in this study were conducted using data from the Human Connectome Project (HCP) (MGH-USC) [8]. The proposed denoising method was applied to DWI datasets with  $b$ -values of 10000  $s/\text{mm}^2$  and 5000  $s/\text{mm}^2$  across three subjects. Comparative performance was assessed against publicly available implementations of MPPCA. Specifically, NYU-MPPCA refers to the implementation by Veraart et al. [1], DIPY-MPPCA refers to the version by Garyfallidis et al. [7]. The adaptive patching variant from the DESIGNER toolbox [6] was also included for fair comparison. Both NYU-MPPCA and DIPY-MPPCA implementations require a fixed kernel size for denoising. In this study, we applied

---

### Algorithm 1 Mapping Gradient Magnitudes to Kernel Sizes for MPPCA

---

**Require:** Gradient magnitude image  $G$  (refer Eq. 1); brain mask  $M$ ; user-specified odd bounds  $k_l, k_u$  with  $k_l \leq k_u$ ; allowable odd integer kernel sizes  $\{n_k\}_{k=1}^K \subseteq [k_l, k_u]$

**Ensure:** Kernel size map  $\mathcal{K}$  (same size as  $G$ ), odd and isotropic

- 1:  $\mathcal{K}_{\text{vals}} \leftarrow \{k \in \mathbb{N} \mid k_l \leq k \leq k_u, k \text{ odd}\} \triangleright$  Allowed odd kernel sizes
- 2:  $K \leftarrow |\mathcal{K}_{\text{vals}}|$
- 3:  $H \leftarrow k_u \triangleright$  Outside-brain kernel size
- 4:  $\mathcal{S} \leftarrow \{G(\mathbf{r}) \mid \mathbf{r} \in \Omega, M(\mathbf{r}) = 1\} \triangleright$  Gradients inside brain
- 5:  $\{\mathcal{C}_i\}_{i=1}^K \leftarrow \text{k-means}(\mathcal{S}, K) \triangleright$  Cluster gradients into  $K$  groups
- 6:  $\mu_i \leftarrow \frac{1}{|\mathcal{C}_i|} \sum_{g \in \mathcal{C}_i} g \text{ for } i = 1, \dots, K \triangleright$  Cluster means
- 7: Compute permutation  $\pi$  such that  $\mu_{\pi(1)} \geq \mu_{\pi(2)} \geq \dots \geq \mu_{\pi(K)} \triangleright$  Higher gradients first
- 8: Sort  $\mathcal{K}_{\text{vals}}$  increasingly:  $k_{(1)} < k_{(2)} < \dots < k_{(K)} \triangleright$  Smaller kernels mapped to higher gradients
- 9: **for all**  $\mathbf{r} \in \Omega$  **do**
- 10:   **if**  $M(\mathbf{r}) = 1$  **then**
- 11:      $g \leftarrow G(\mathbf{r})$
- 12:     Find  $i \in \{1, \dots, K\}$  such that  $g \in \mathcal{C}_{\pi(i)}$
- 13:      $\mathcal{K}(\mathbf{r}) \leftarrow k_{(i)} \triangleright$  Monotonic mapping: high  $G \rightarrow$  small  $k$
- 14:   **else**
- 15:      $\mathcal{K}(\mathbf{r}) \leftarrow H \triangleright$  Outside brain: assign  $k_u$
- 16:   **end if**
- 17: **end for**
- 18: **return**  $\mathcal{K}$

---

isotropic kernel sizes of 5, 7, and 9 for these two methods. For the proposed ak-MPPCA, the kernel size estimation limits were set to [5, 9].

## 3. RESULTS AND DISCUSSION

Three subjects from the HCP (MGH-USC) dataset [8] were analyzed: MGH-1005, MGH-1006, MGH-1010. Denoised DWI results are shown in Figure 1. For MGH-1010 and MGH-1006, DWI data with  $b = 10000 \text{ s}/\text{mm}^2$  was used, while for MGH-1005, results are shown for  $b = 5000 \text{ s}/\text{mm}^2$ . The primary diffusion directions for the noisy and denoised (using proposed method) DWI data are represented using a red-green-blue representation to create a directionally encoded color (DEC) map (color FA maps) in Figure 2 [7, 9]. As shown in Figure 1, the NYU-MPPCA and DIPY-MPPCA denoised DWI data depends on the kernel size choice (a hyperparameter to be optimized). In contrast, the proposed method estimates voxel-wise kernel sizes based on local structural information (refer Section 2.1). The corresponding kernel size maps are also shown in Figure 1. These maps reveal that

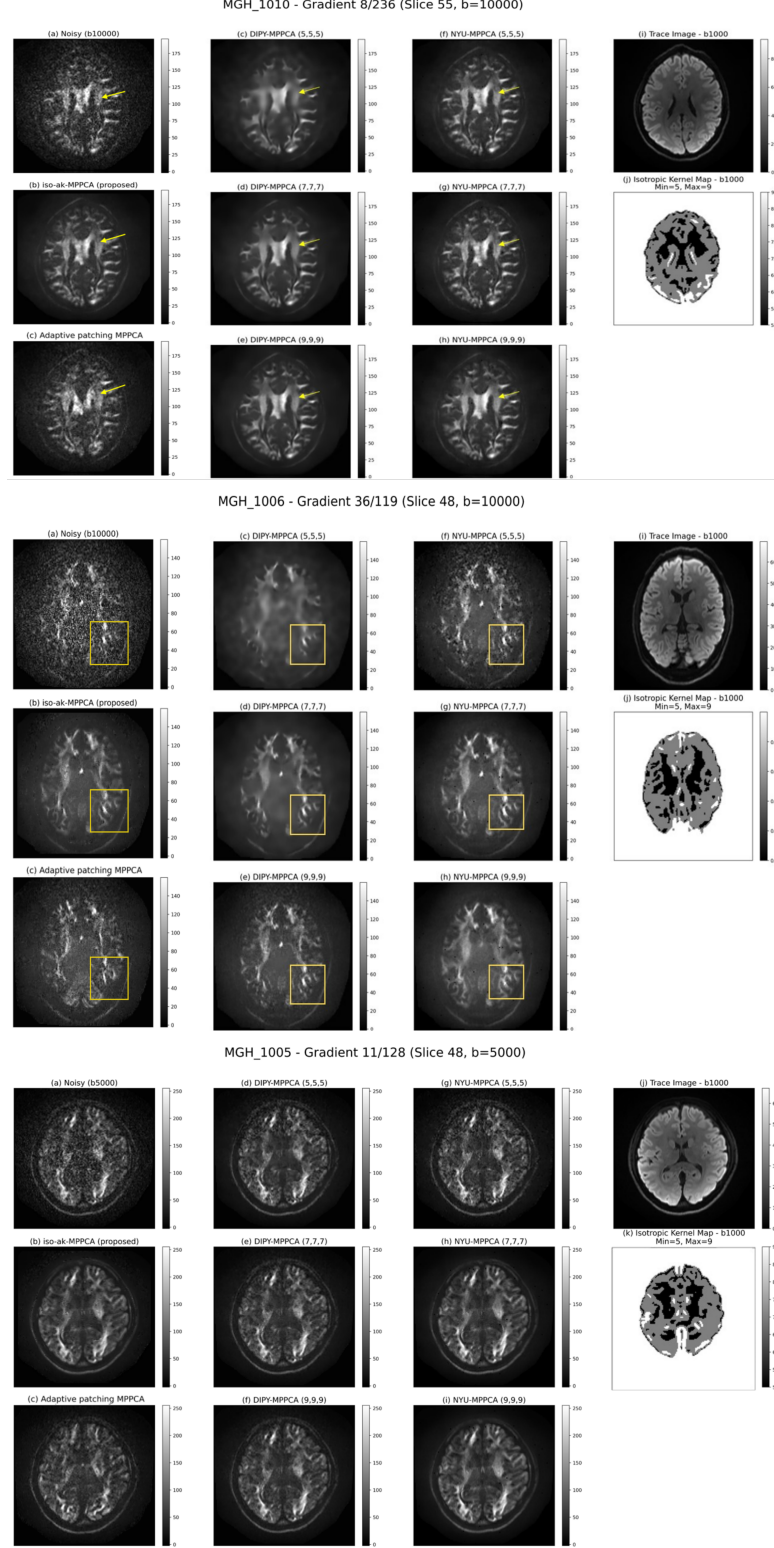


**Fig. 1.** Visual comparison of denoising results across methods for each subject. Panels show: (a) original noisy DWI image, (b) denoised image using the proposed ak-MPPCA method, (c) adaptive patching MPPCA [6], (d–f) DIPY-MPPCA [7] with varying kernel sizes, (g–i) NYU-MPPCA [1] with varying kernel sizes, (j) trace image used for kernel size estimation (see Section 2.1.1), and (k) voxel-wise kernel size map generated using Algorithm 1. The kernel map in (k) was used to guide MPPCA denoising in (b). Yellow arrows/boxes highlight regions where the proposed method demonstrates improved preservation of structural detail and reduced blurring compared to other approaches (without requiring any kernel size adjustments).

regions with high structural detail are assigned smaller kernel sizes, helping preserve fine features and reducing the risk of blurring during denoising. Although the adaptive patching MPPCA [6] addresses structural blurring to some extent, it does not suppress noise as effectively. Among the compared methods, the proposed approach demonstrates superior performance in preserving anatomical structure while effectively reducing noise in DWI data. As observed from the color FA maps in Figure 2, the proposed method improves the clarity of these maps, resolving noisy regions and preserving meaningful diffusion direction information.

#### 4. CONCLUSION

We proposed ak-MPPCA, a denoising method for DWI that estimates voxel-wise kernel sizes based on local image gradients. Unlike fixed-size MPPCA methods [1, 7], ak-MPPCA adapts to structural complexity, improving noise reduction and detail preservation. Evaluated on high b-value data from the HCP [8], ak-MPPCA performed better than existing approaches, including adaptive patching [6], in producing cleaner DWI and more accurate color FA maps.

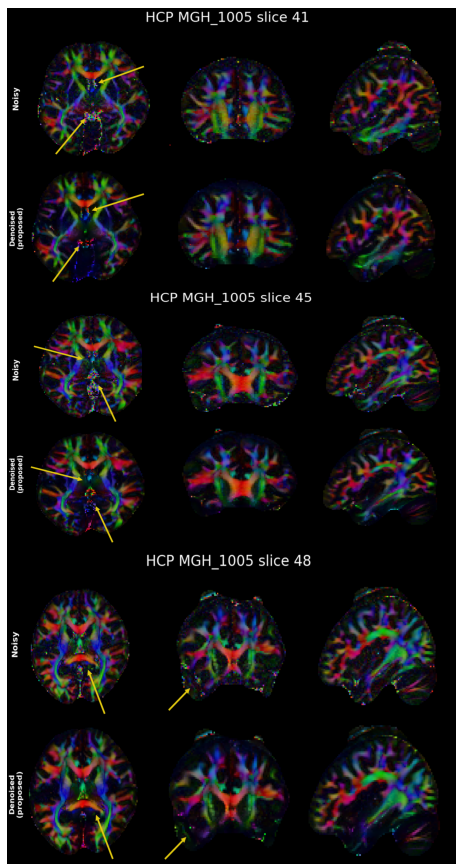


**Fig. 2.** The primary diffusion directions for the noisy and ak-MPPCA denoised DWI data are shown color FA maps [9, 7]. The proposed method improves the clarity of these maps.

#### 5. REFERENCES

- [1] J. Veraart, D.S. Novikov, D. Christiaens, B. Ades-Aron, J. Sijbers, and E. Fieremans, “Denoising of diffusion mri using random matrix theory,” *Neuroimage*, vol. 142, pp. 394–406, 2016.
- [2] R.N. Henriques, A. Ianuş, L. Novello, J. Jovicich, S.N. Jespersen, and N. Shemesh, “Efficient pca denoising of spatially correlated redundant mri data,” *Imaging Neuroscience*, vol. 1, pp. 1–26, 2023.
- [3] J.L. Olesen, A. Ianus, L. Østergaard, N. Shemesh, and S.N. Jespersen, “Tensor denoising of multidimensional mri data,” *Magnetic Resonance in Medicine*, vol. 89, no. 3, pp. 1160–1172, 2023.
- [4] H. Herthum and S. Hetzer, “Tensor denoising of quantitative multi-parameter mapping,” *Magnetic Resonance in Medicine*, vol. 92, no. 1, pp. 145–157, 2024.
- [5] Benjamin Ades-Aron, Jelle Veraart, Peter Kochunov, Stephen McGuire, Paul Sherman, Elias Kellner, Dmitry S Novikov, and Els Fieremans, “Evaluation of the accuracy and precision of the diffusion parameter estimation with gibbs and noise removal pipeline,” *Neuroimage*, vol. 183, pp. 532–543, 2018.
- [6] Jenny Chen, Benjamin Ades-Aron, Hong-Hsi Lee, Subah Mehrin, Michelle Pang, Dmitry S Novikov, Jelle Veraart, and Els Fieremans, “Optimization and validation of the designer preprocessing pipeline for clinical diffusion mri in white matter aging,” *Imaging Neuroscience*, vol. 2, pp. 1–17, 2024.
- [7] Eleftherios Garyfallidis, Matthew Brett, Bagrat Amirbekian, Ariel Rokem, Stefan Van Der Walt, Maxime Descoteaux, Ian Nimmo-Smith, and Dipy Contributors, “Dipy, a library for the analysis of diffusion mri data,” *Frontiers in neuroinformatics*, vol. 8, pp. 8, 2014.
- [8] Qiuyun Fan, Thomas Witzel, Aapo Nummenmaa, Koene RA Van Dijk, John D Van Horn, Michelle K Drews, Leah H Somerville, Margaret A Sheridan, Rosario M Santillana, Jenna Snyder, et al., “Mgh-usc human connectome project datasets with ultra-high b-value diffusion mri,” *Neuroimage*, vol. 124, pp. 1108–1114, 2016.
- [9] Sinisa Pajevic and Carlo Pierpaoli, “Color schemes to represent the orientation of anisotropic tissues from diffusion tensor data: application to white matter fiber tract mapping in the human brain,” *Magnetic Resonance in Medicine: An Official Journal of the International Society for Magnetic Resonance in Medicine*, vol. 42, no. 3, pp. 526–540, 1999.